Talanta 184 (2018) 475–483

Contents lists available at ScienceDirect

Talanta

journal homepage: www.elsevier.com/locate/talanta

Direct E-DNA sensor of Mycobacterium tuberculosis mutant strain based on new nanocomposite transducer (Fc-ac-OMPA/MWCNTs)

Salma Bizid[a,b], Saber Blili[a], Rym Mlika[a,*], Ayoub Haj Said[a], Hafsa Korri-Youssoufi[b]

[a] Laboratory of Interfaces and Advanced Materials, Faculty of Science of Monastir, University of Monastir, 5019 Monastir, Tunisia
[b] UMR-CNRS, Institute of Molecular Chemistry and Materials of Orsay, Bioorganic and Bioinorganic Chemistry Team, University Paris-Sud, Building 420, 91405 Orsay, France

ARTICLE INFO

Keywords:
Redox oligomer
Poly(p-phenylene)
MWCNTs
Electrochemistry
DNA biosensor

ABSTRACT

Direct DNA sensor based on new nanocomposite materials (Fc-ac-OMPA/MWCNTs) has been investigated. This nanocomposite was formed by combining the redox oligomer "oligo-methoxy-phenyl-acetonitrile" (Fc-ac-OMPA) and the MWCNTs via a simple π-π stacking interaction in the aim to ameliorate the biosensor performance. The redox indicator and the functional groups of the redox oligomer have been used for monitoring the electrochemical behavior and the flexibility for direct covalent attachment of Hepatitis C DNA probe. This nanocomposite shows high performance of DNA hybridization with a detection limit of 0.08 fmol L^{-1}. Moreover, the biosensor was applied for the detection of pathogenic bacterium such as DNA from *Mycobacterium tuberculosis* strand. Developed biosensor has been able to detect a single nucleotide polymorphism (SNP)T (TCG/TTG) which confers resistance of M. tuberculosis to rifampicin drug.

1. Introduction

Mycobacterium tuberculosis (*M. tuberculosis*) is a dangerous pathogenic bacterium that is one of the major causes of pulmonary tuberculosis and remains the second leading cause of death from an infectious disease worldwide [1,2]. The Rapid and sensitive detection methods for *M. tuberculosis* represents a major challenge for scientists. The common method used for diagnosing *M. tuberculosis* is sputum smear microscopy, however, it's not a rapid and a sensitive method [3,4] which limits its value in the case of a rapid diagnosis. Various molecular diagnostic methods, such as real-time polymerase chain reaction (PCR), DNA microarray assay and cycling probe technology, have been developed to detect Mycobacteria nucleic acids in sputum or culture samples [5–7]. Even though, these diagnostic methods have high specificity and sensitivity, most of them are still limited by cost, time and require specialized expensive fabrication protocols [8,9] that are not able to provide low-cost, miniature, portable devices for real-time genomic DNA detection. Thus, there is a need to develop specialized DNA hybridization platforms able to perform highly sensitive and specific direct analysis [10]. Indeed, the combination of PCR amplification with electrochemical devices provides a sensitive method for specific sequence detection [11]. Actually, electrochemical sensors have shown great potential in providing viable solutions to this challenge. This analytical method is faster, low cost, simple to fabricate and can be miniaturized [12,13]. These advantages make electrochemical sensors an appropriate application tool for DNA detection [14]. The sensitivity and lifetime of DNA sensors depend on the immobilization of DNA probes onto the electrochemical transducer. The immobilization of DNA probes can be presented in different methods, including electrochemical polymerization [15], self-assembled methods [16] and covalent binding [17]. One of the promising approaches is covalent bonding between the nucleic acid system and electroactive polymers [18,19]. These electroactive polymers are taking researchers' attention not only because they have excellent electrical properties and high stability, but also, and most important thing they do not require the addition of an extra redox active compound [20]. This type of redox polymer can directly report the hybridization event with improved sensitivity [21,22]. In addition, a lot of nanomaterials, such as carbon nanomaterials, have been explored as a perfect transducer since they have the ability to amplify the signal transduction [23]. They have been widely recognized as an ideal support for fabricating electrochemical sensors [24,25]. DNA biosensors based on a hybrid composite of CNTs and electroactive polymers have received significant interest because the combination of these composite materials, maintains the properties of each component with a synergistic effect [26,27]. In fact, these nanomaterials (MWCNTs) and the redox polymer can be associated through a simple π-π stacking interaction [28] that can promote electron transfer reactions. Additionally, having a high surface area increases

* Corresponding author.
E-mail address: mlikarym@yahoo.fr (R. Mlika).

https://doi.org/10.1016/j.talanta.2018.03.025
Received 15 January 2018; Received in revised form 8 March 2018; Accepted 10 March 2018
Available online 14 March 2018
0039-9140/

dramatically the amount of DNA probe attachment and the overall hybridization sensitivity [29].

In this paper, we report the direct detection of DNA hybridization using electrochemical biosensors based on (MWCNTs) and redox polymer. The gold electrode surface was modified with the nanocomposite layer (Fc-ac-OMPA/MWCNTs) as a platform for the immobilization of Hepatitis C DNA probe. The most striking point of this work is the ease of construction of the biosensor through the direct covalent bonding between the DNA and the nanocomposite rich in carboxylic groups from the structure of the oligomer (Fc-ac-OMPA). Further, the hybridization of complementary target (c DNA) at different concentrations from 1 fmol L^{-1} to 1 nmol L^{-1} has been investigated by CV via ferrocene. The sensitivity of this biosensor is enhanced by combining the high electrical conductivity of MWCNTs with the electrical properties of Fc-ac-OMPA. The present biosensor demonstrates the ability for sensing DNA of the rpoB gene of *Mycobacterium tuberculosis* in real PCR samples.

2. Material and methods

2.1. Materials

The redox oligomer "oligo-methoxy-phenyl-acetonitrile" "Fc-acid-OMPA" (Fc-ac-OMPA) has been synthesized and characterized according to the previously reported procedure [22,30]. Multiwalled carbon nanotubes (MWCNTs) obtained commercially from Baytubes has a diameter that varies between 5 and 20 nm with a length of over 1 μm. The nanocomposite solvent used was Chloroform ($CHCl_3$) and has been purchased from Sigma-Aldrich. The electrolyte used for electrochemical analysis is an aqueous solution of lithium perchlorate 0.1 mol L^{-1} $LiClO_4$ (pH = 7) at room temperature. Phosphate buffer saline (PBS) (10 m mol L^{-1}, pH = 7.4) has been filtered through 0.22 μm pore size membrane. All the prepared solution has been stored at 4 °C until use.

Synthetic DNA sequences of Hepatitis C have been provided by Eurogentec Company (Eurogentec, Liège, Belgium):

- The DNA probe: NH_2-$(CH_2)_6$ −5′GAT-ACT-TCT-ATC-ACC-CAT3′ (18-bases sequences with six carbon chains (C6) as spacer and with amine group on its 5′ phosphoryl terminus).
- The complementary target (c DNA): 5′CTA-TGA-AGA-TAG-TGG-GTA3′.
- The non-complementary target (nc DNA): 5′ATG-TGG-TAG-AGA-TGA-CTA3′.

The PCR samples of *Mycobacterium Tuberculosis* genomic DNA has been obtained from "laboratory I2BC" of Prof C. Sola team from the University of Paris-Sud. The DNA probes, specific to the wild stand and mutant of *Mycobacterium tuberculosis* PCR, are containing 18 bases with 5′ terminal amino group modification uses a twelve carbonyl chain spacer (C12) with the sequences of the wild type are 5′-CCGA CTG(T**C**G)GCGCT-GGG-3′ and the mutated type are 5′-CCGACTG(T**T**G) GCGCTGGG-3′ [31]. A stage of 35 cycles PCR has been made on the DNA crud to amplify the sequences which correspond to the rpob gene using various cycles of temperatures and two primers: a forward primer with TR1 (5′-TACGGTCGGCGAGCTGATCC-3′) and a reverse primer with TR2 (5′-TACGGCGTTTCGATGAACC-3′) [32]. The obtained DNA from PCR contains 411 bases. The concentration has been measured following absorbance by Nanodrop 1000. All the solutions have been stored at 20 °C until use [22].

2.2. Instrumentations

The *UV–Visible Spectroscopy* has been recorded with spectrophotometer Cary Varian using a 100 μL quartz cell.

Scanning Electron Microscopy (SEM) technique was used to evaluate the surface morphology of the film deposited on gold substrate by spin-coating. SEM images were performed with a Hitachi scanning electronic microscope (SEM 4800).

The sessile drop method *contact angle measurements* using a GBX Scientific Instrument has been used to observe hydrophobicity and adhesion of the deposited membrane on gold surfaces. Van Oss theoretical model has been used with three solutions: diiodomethane, formamide and deionised water as probes for the surface energy calculations.

X-Ray photoelectron spectrometry (XPS) measurements were performed on a K Alpha spectrometer from Thermofisher, using a monochromated X-ray Source (Al Kα, 1486.6 eV). The spectrums obtained were treated by means of the "Avantage" software provided by Thermofisher. Shirley type background subtractions were used.

Electrochemical Impedance Spectroscopy (EIS) and cyclic voltammetry (CV) have been used via a Metrohm potensiostat Autolab (PGSTAT 20) supported by Nova software. The electrochemical measurements were carried out in a three-electrode system: a platinum mesh as a counter electrode, an Ag/AgCl as a reference electrode and a gold disc (surface 2.01 $\times 10^{-2}$ cm^2) as a working electrode. Cyclic Voltammetry have been realized with the scan rate of 50 mV s^{-1} by cycling the potential from 0 V to 0.9 V. Electrochemical Impedance Spectroscopy measurements has been performed with a sinusoidal excitation signal of 10 mV amplitude and a frequency range of 100 kHz to 100 mHz at 0.45 V vs Ag/AgCl.

2.3. Biosensor construction

The proceeded method of the nanocomposite preparation (Fc-ac-OMPA/MWCNTs) is made by a direct mixing of the MWCNTs and the redox oligomer in a suitable solvent. In this work, the nanocomposite has been prepared by mixing 5 mg of Fc-ac-OMPA oligomer and 0.2 mg of MWCNTs (4%) in 1.5 ml solution of chloroform ($CHCl_3$). The dispersion has been conducted by sonication during one hour.

After the polishing steps of the gold surface, the first step of the biolayer construction was the deposition of 5 μL of the prepared nanocomposite solution (Fc-acid-OMPA/MWCNTs) and then letting them to dry at room temperature during one night. For the biolayer formation, the DNA covalent attachment has been carried out through the acid functions available on the surface of the oligomer layer. The presence of carboxylic acid groups on the transducer is necessary for covalent bonding of oligonucleotides when using standard carbodiimide chemistry. The electrode was then dipped during 45 min in the solution formed by EDC/NHS (20 m mol L^{-1}) and DNA probe (10 μ mol L^{-1}) in PBS buffer pH = 7.4 at room temperature. EDC/NHS forms a reactive intermediate during the formation of amide bonds between the carboxylic acids of the oligomer and the amino-terminal end of the oligonucleotides. To saturate the non-bonded activated carboxylic acid groups, the electrode has been immersed in 1 μmol L^{-1} of ethanolamine (EtOH) solution in a PBS buffer for 30 min at room temperature. Then, this formed biosensor was carefully washed with double-distilled water and stored in PBS buffer at 4 °C until use. A various concentration of DNA target ranges from 1 fmol L^{-1} to 1 nmol L^{-1} prepared in PBS buffer solution was used for the hybridization step at 40 °C for 1 h. After each incubation, the electrode has been then washed with double-distilled water. The biosensor construction was controlled by CV and EIS measurement in aqueous solution (0.1 mol L^{-1} $LiClO_4$, pH = 7). Scheme 1 summarizes the different steps of the biolayer construction and DNA interactions on the nanocomposite film (Fc-acid-OMPA/MWCNTs).

3. Results and discussion

3.1. Nanocomposite (Fc-acid-OMPA/MWCNTs) characterizations

Earlier studies suggested that polymer containing an aromatic ring,

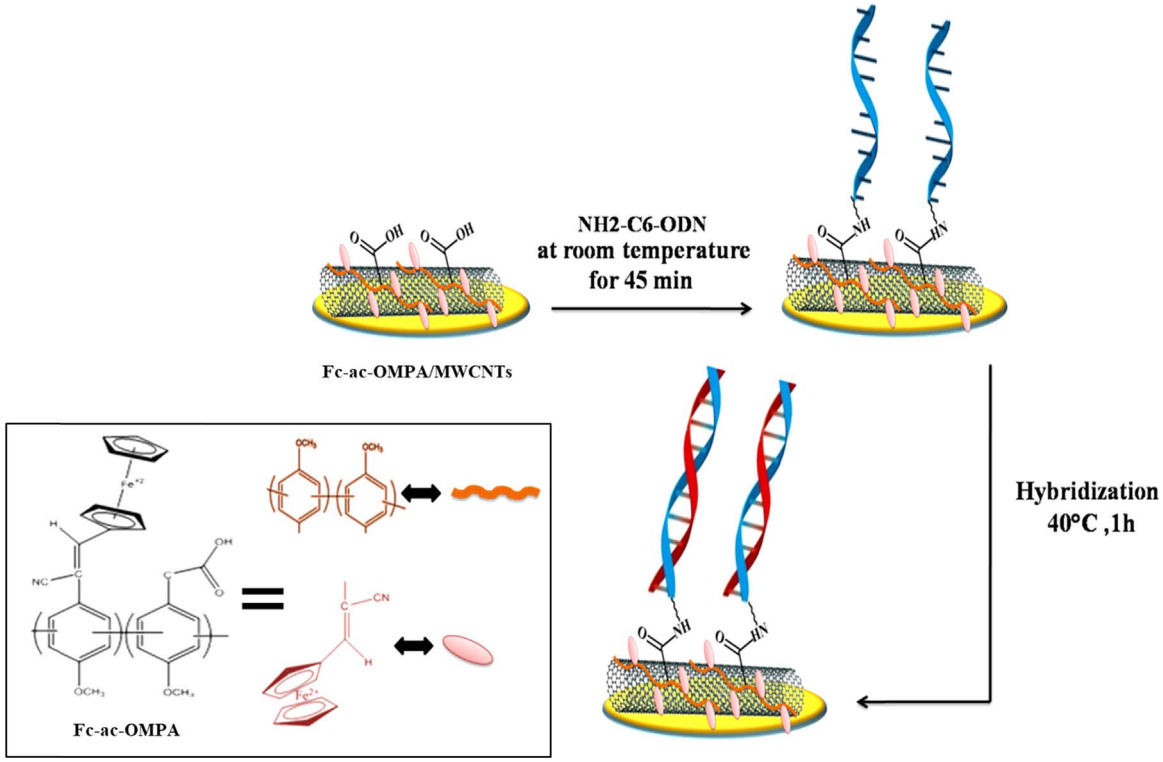

Scheme 1. The biolayer formation on the nanocomposite transducer, the first step is the covalent attachment of DNA through amide link in the presence of coupling agent (EDC)/(NHS). The second step is hybridization reaction with DNA complementary target.

could have strong interaction with CNTs via π-π stacking [33]. In fact, the CNTs exhibit a special sidewall curvature and possessing a π-conjugative structure with a highly hydrophobic surface. These exceptional properties of the CNTs allow them to interact with many organic compounds, aromatic compounds, in particular, through π-π electronic and hydrophobic interactions [34]. Therefore, it concluded that the delocalization of π conduction electrons between nanotubes and a polymer containing an aromatic ring result in the adsorbtion of the polymer onto the CNTs surface [33]. As a result, this strong interaction between polymer and CNTs could form a new nanostructure, as demonstrated previously [34,35].

Since Fc-ac-OMPA is a typical aromatic polymer, the π-π stacking interactions with the MWCNTs could be observed by UV–Vis spectroscopy. Fig. 1 shows the UV spectra of Fc-ac-OMPA with a characteristic absorption band around 325 nm attributed to the π-π* transition of the conjugated oligophenylene backbone and a second band at 491 nm assigned to the ferrocene moiety [30]. Mixing the oligomer with the MWCNTs conduct to an increase in this band intensity with a slight red shift (~5 nm), as observed in Fig. 1. This rise in absorption of the π-π* transition bands indicate a strong π-π stacking interactions between the π-electron of the Fc-ac-OMPA aromatic rings and the π-conjugated of the MWCNTs surfaces [36,37].

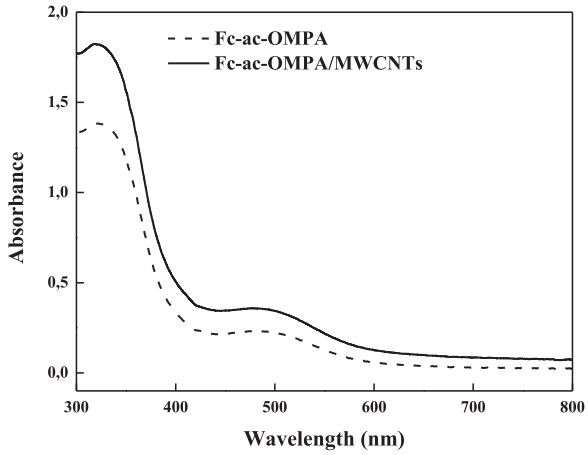

Fig. 1. UV–Visible spectra of the nanocomposite Fc-ac-OMPA/MWCNTs and Fc-ac-OMPA oligomer in chloroform solution dissolved at concentration of 1 mg /0.1 ml.

This result was also confirmed by the surface characterization of the nanocomposite film through SEM and wettability techniques. Fig. 2A shows the SEM images of the unmodified MWCNTs. Fig. 2B and C show SEM images of the redox oligomer alone and the nanocomposite membrane deposited on the gold surfaces. Comparing Fig. 2A with Fig. 2B and Fig. 2C reveals that the polymer has been dispersed with the nanotubes and filled the empty voids between individual nanotubes. The images reveal a difference of contrast with an inhomogeneous surface with the presence of MWCNTs filament randomly distributed across the membrane, as shown in Fig. 2C. Furthermore, the SEM image (Fig. 2D) shows an increase in the diameter of the CNTs dispersed with the Fc-OMPA polymer (~18 nm) with respect to the diameter value of the CNTs alone (~5 nm) [38]. This confirms the good adsorption of the Fc-ac-OMPA onto MWCNTs interface by π-π stacking interactions. It is also possible to notice in the 45° inclined image the presence of the CNTs and the (Fc-acid-OMPA/MWCNTs) dispersed in the volume of the membrane surface (Fig. 2E).

In addition, we noticed that the hydrophobicity of the nanocomposite film increased slightly to a value of θ = 87.2° compared to a value of θ = 82.6° for Fc-ac-OMPA. Also, we perceived a better surface energy with the nanocomposite surface (γ_S = 55.4 mJ/m^2) compared to the pure oligomer (γ_S = 45.6 mJ/m^2). These wettability characteristics confirm the good hydrophobic interactions between the MWCNTs and the Fc-ac-OMPA. Moreover, the increase of the surface energy between the nanocomposite and the gold surface indicate the amelioration of the physical adsorption. These results lead to conclude the formation of a stable nanomaterial.

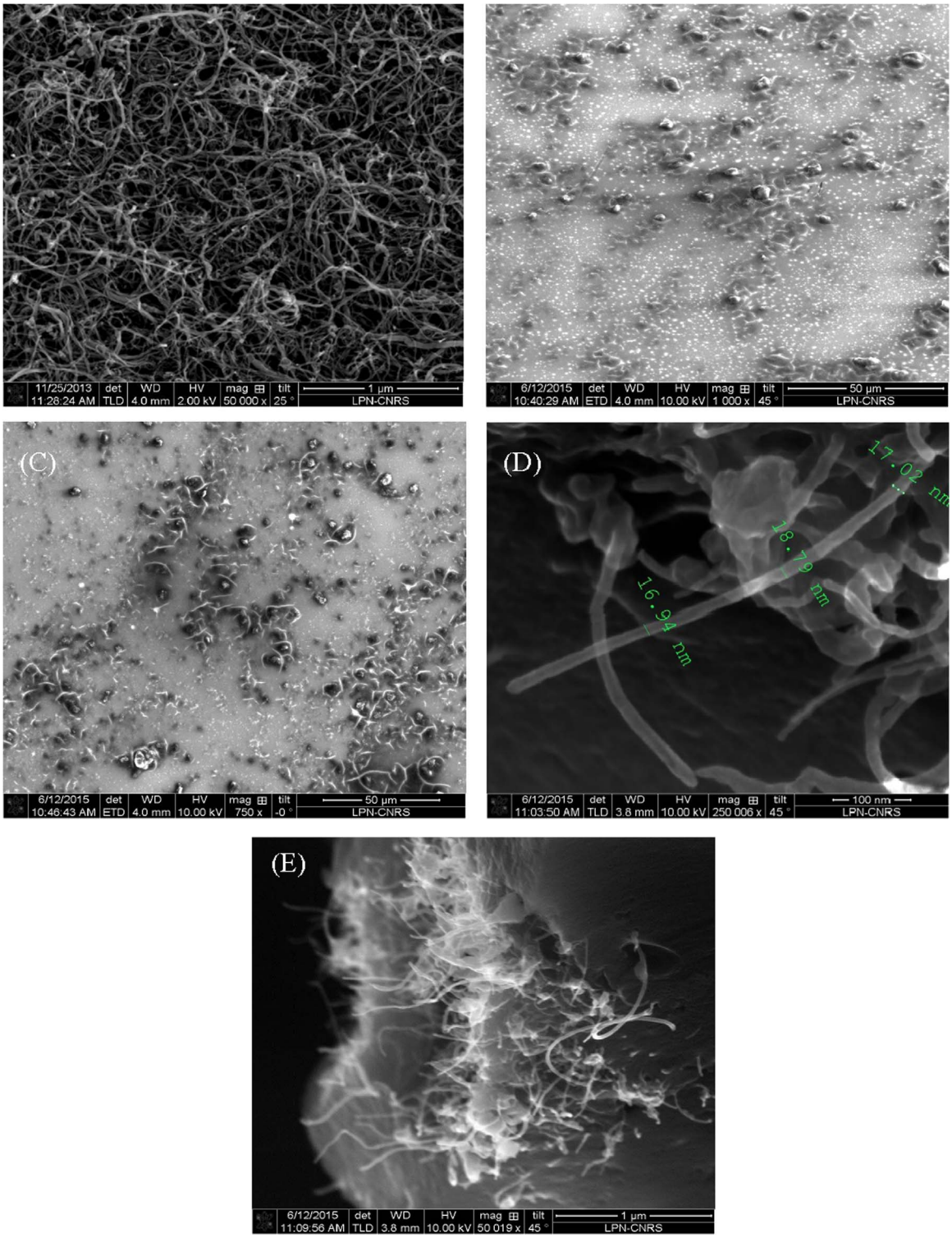

Fig. 2. SEM image of (A) MWCNTs, (B) Fc-ac-OMPA, (C) Fc-ac-OMPA/MWCNTs deposited on gold surface, (D) Diameter of the CNTs dispersed with the oligomer Fc-ac-OMPA (E) Image of Fc-ac-OMPA/MWCNTs at 45°.

3.2. Nanocomposite (Fc-acid-OMPA/MWCNTs) electrochemical study

A cyclic voltammetry study has been carried out on the nanocomposite membrane to study the doping effect of the redox oligomer Fc-ac-OMPA by the MWCNTs on the electron charge transfer kinetics. Fig. 3A shows the CVs superposition of the surface modified with Fc-ac-OMPA and the Fc-ac-OMPA/MWCNTs layer at a scan rate of 50 mV s^{-1}. We can observe that Fc-ac-OMPA/MWCNTs layer exhibits a higher current (Ia = 1.028 × 10^{-5} A) than the pure redox polymer Fc-ac-OMPA (Ia = 2.780 × 10^{-6} A). This result can be explained by the fact that at the level of the nanocomposite membrane the insertion of the CNTs with the oligomer accelerated the charge transfer kinetics [39]. This acceleration is attributed to the high conductivity of carbon nanotubes, which act as a topological bridge for electrons [40].

The surface coverage (Γ) of the nanocomposite modified gold electrode has been calculated as follows: $\Gamma = \frac{Q}{nFA}$

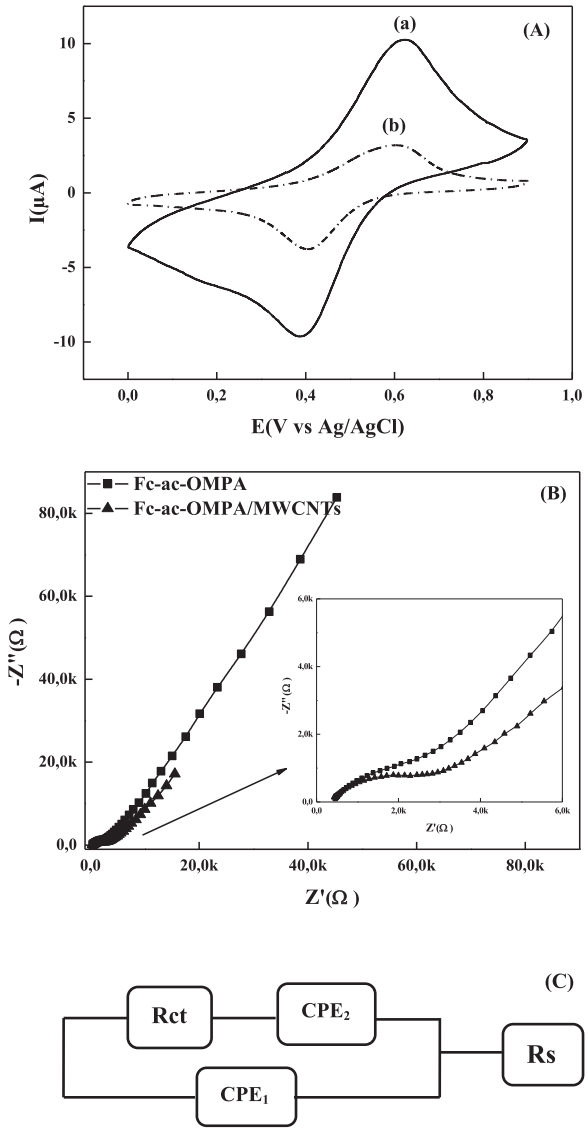

Fig. 3. (A) Curve (a) present CV of nanocomposite layer (Fc-ac-OMPA/MWCNTs) compared to curve (b) of pure polymer layer (Fc-ac-OMPA), recorded in solution LiClO4 (0.1 M, pH = 7) at scan rate of 50 mV s^{-1}. (B) Nyquist plots of (■) Fc-ac-OMPA and (▲) Fc-ac-OMPA/MWCNTs recorded at 0.45 V vs. Ag/AgCl in LiClO4 (0.1 M, pH = 7) at ac potential of 10 mV in the frequency range of 100 kHz to 100 mHz. Right is the zoom of diagram at lower frequency range. Symbol represents the experimental data and solid line represents the fitted data obtained with the equivalent circuit shown below. (C) Equivalent circuit model.

Where n is the number of electrons involved in the redox reaction ($n = 1$), Q is the charge under the oxidation peak, A is the gold electrode area (2.01×10^{-2} cm^2) and F is the Faraday constant (96485 C/mol). The calculated surface coverage (Γ) ratio of nanocomposite membrane equals to $\Gamma = (1.54 \pm 0.032\ 10^{-6})$ mol cm^{-2}. This value is higher than that of the polymeric membrane ($\Gamma = (4.55 \pm 0.12\ 10^{-7})$ mol cm^{-2}). This is due to the large surface area of the CNTs thus promoting interaction with the oligomer.

These previous results have been confirmed by electrochemical impedance spectroscopy analyses. Fig. 3B shows the Nyquist diagram of the pure redox oligomer (Fc-ac-OMPA) and the nanocomposite (Fc-ac-OMPA/MWCNTs). The experimental results have been fitted with Randles equivalent circuit [41] presented in Fig. 3C. The equivalent circuit formed by the electrolyte resistance (R_s), the charge transfer resistance at the membrane/electrode interface (R_{ct}), the constant phase element (CPE_1) represents the double layer capacity and the constant phase element (CPE_2) is related to the space charge capacity in the polymer membrane. The fit results have been summarized in Table 1. From the result obtained by the fit, we have observed that the value of the charge transfer resistance for the nanocomposite membrane (Rct = 3.54 kΩ) is lower than that of the pure redox oligomer (Rc = 6.05 kΩ). Thus, it can be concluded that the doping of the redox oligomer by the carbon nanotubes has improved the transfer of electronic charge at the membrane/electrode interface.

Table 1
Fitting parameters circuit of Fc-acid-OMPA/MWCNTs membrane and biolayer construction.

	Fc-ac-OMPA/ MWCNTs	Fc-ac-OMPA/ MWCNTs +ADN	+ 1 nM cDNA	+ 1 nM ncDNA
Rs (Ω)	333.3	321.3	425.1	312.9
(RDS%)	(0.63%)	(0.40%)	(0.24%)	(0.36%)
CPE_2(µF)	Q = 4.483	Q = 2.046	Q = 1.422	Q = 2.619
(RDS%)	(0.25%)	(1.43%)	(0.10%)	(1.11%)
	n = 0.54	n = 0.60	n = 0.76	n = 0.59
	(0.5%)	(0.5%)	(0.5%)	(0.5%)
R_{ct} (kΩ)	3.54	23.56	309.18	46.32
(RDS%)	(3.97%)	(3.71%)	(2.93%)	(2.33%)
CPE_1(µF)	Q= 55.46	Q= 34.85	Q = 3.601	Q = 23.46
(RDS%)	(0.24%)	(2.05%)	(1.59%)	(4.81%)
	n = 0.61	n = 0.60	n = 0.46	n = 0.56
	(0.5%)	(0.5%)	(0.5%)	(0.5%)
χ^2	0.078	0.060	0.26	0.035

Moreover, a kinetic study has been carried out by nanocomposite membrane analysis at different scanning speeds from 10 mV s^{-1} to 500 mV s^{-1} with a potential range from 0 V to 0.9 V. The variation of the peaks versus the scan rate or the root of the scan rate gives the same behavior observed with the pure redox oligomer Fc-ac-OMPA [22]. Where the peaks' current at a lower speed varies linearly with the scan rate and then at a higher speed the current varies linearly with the root of scan rate. This behavior underlines that both electron transfer and ionic transfer relate to the diffusion of ions through the nanocomposite membrane and the control of the electrochemical process (See Supplementary data). Through this analysis, the electron transfer rate constant (ks) can be determined using the equation developed by Laviron: $ks = \frac{mnvF}{RT}$

Where m is determined by the adjustment of the curve ΔEp = f (m^{-1}) [22,42] R is the universal gas constant (8.31 J mol^{-1} K^{-1}), T is absolute temperature (298 K), n is the number of electrons involved in the redox reaction ($n = 1$), F is the Faraday constant (96485 C mol^{-1}), and v is the scan rate.

Comparing the ks value of the pure redox oligomer ks = (6.43 ± 0.19) s^{-1} to the nanocomposite ks = (7.79 ± 0.15) s^{-1}, we can observe that the constant ks has increased, indicating that the transfer of charges takes place more rapidly through the nanocomposite membrane.

3.3. Application of the nanocomposite membrane as a transducer for DNA detection

The resulting nanocomposite material has been applied as a transducer in the construction of the DNA sensor. The preparation of the biosensor, as described previously (Section 2.3), consisted of covalent attachment of single-stranded DNA probe (ssDNA), constituted of 15 bases modified with the amine group on 5′ end, to the acid functions available on the oligomer layer through an amide link. The formation of the electrochemical biosensor was monitored by both cyclic voltammetry (CV) and impedance spectroscopy (EIS) in $LiClO_4$ (0.1 mol L^{-1}, pH = 7). The grafting of the DNA probe has been carried out in a PBS solution (pH = 7.4) for 45 min at room temperature and then analyzed by CV with a scan rate of 50 mV s^{-1}. The ferrocene groups will allow seeing the follow-up of the electrochemical response during the construction of the biosensor. We noted that the intensity of the redox

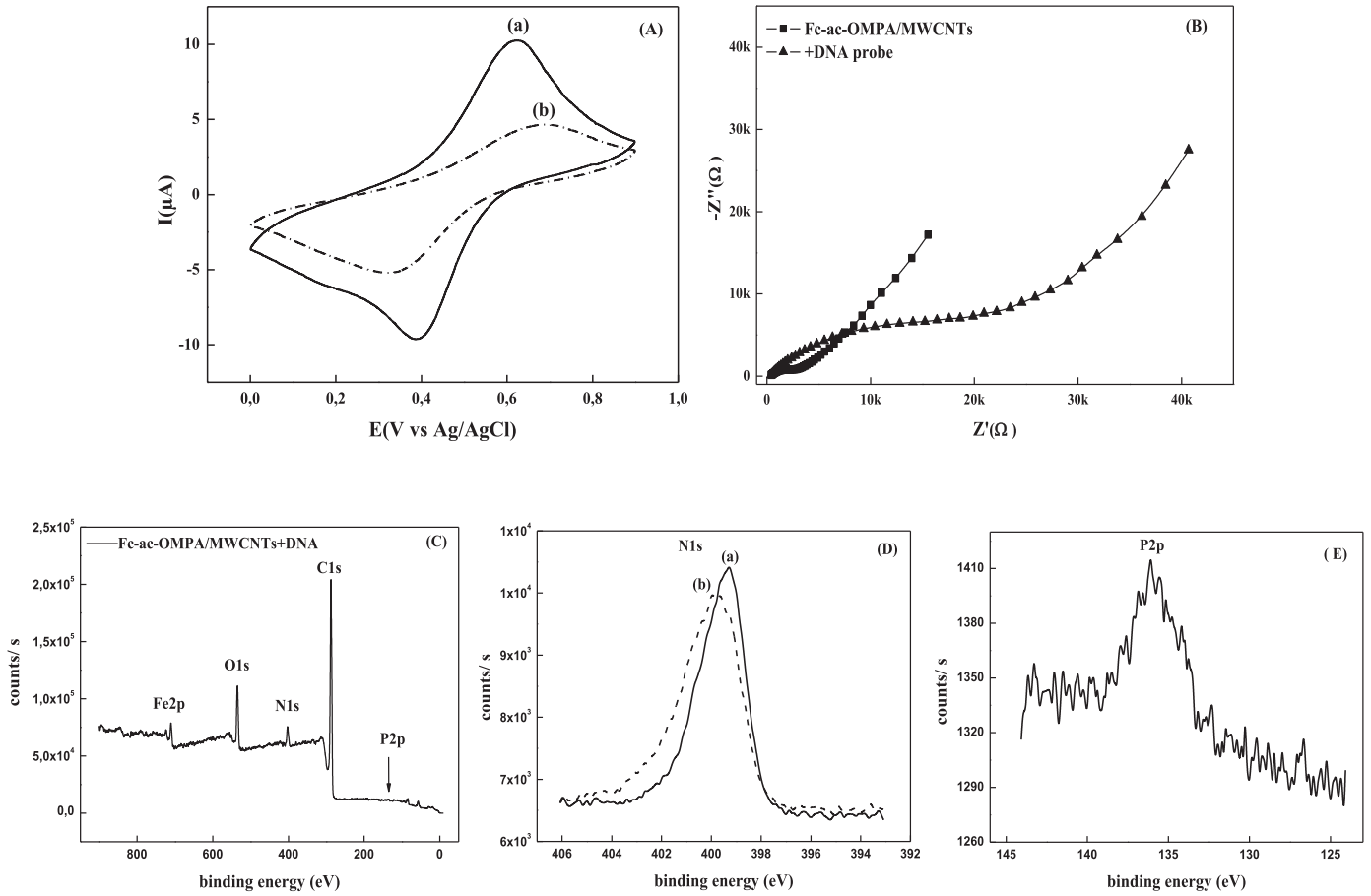

Fig. 4. (A) CV data obtained after biosensor formation: curve (a) Fc-ac-OMPA/MWCNTs, curve (b) Fc-ac-OMPA/MWCNTs + DNA. The immobilization of DNA was performed in PBS (pH = 7.4) during 45 min at room temperature. The CVs are recorded in 0.1 M LiClO4 (pH = 7) with scan rate of 50 mV s^{-1}. (B) Nyquist plots of the biolayer construction recorded at 0.45 V vs Ag/AgCl at Dc potential of 10 mV in the frequency range of 100 kHz to 100 mHz. (■) Fc-ac-OMPA/MWCNTs, (▲) Fc-ac-OMPA/MWCNTs + DNA. The points presenting the experimental data and the line is the fit obtained with the equivalent circuit. (C) XPS spectra of Fc-ac-OMPA/MWCNTs + DNA, (D) N1s spectra, curve (a) Fc-ac-OMPA/MWCNTs, curve (b) Fc-ac-OMPA/MWCNTs + DNA, (E) P2p spectra.

centers (ferrocene) decreased and a slight shift of the peaks towards the positive potentials (from 0.62 V to 0.69 V) is noticed after the biosensor construction (Fig. 4A). This is related to the immobilization of the DNA molecule on the surface that affects the charge transfer of the redox centers [20,43]. Also the rate of the surface coverage after the grafting of the biolayer decreased with a value of $\Gamma = (7.41 \pm 0.27)\ 10^{-7}$ mol cm^{-2}. This coverage decrease proves the good attachment of the biological molecule on the surface. These results have been also confirmed by EIS (Fig. 4B), where we observed an increase of the resistance Rct = 23.56 kΩ (Table 1). Which can confirm the interaction of the DNA chain with the nanocomposite membrane, that leads to changes in the electronic properties of the transducer [44].

To demonstrate the efficiency of the DNA probe attachment on the Fc-ac-OMPA/MWCNTs layer, XPS analyses have been performed. Firstly, a spectrum has been made over a wide range of energy to detect chemical elements present in the Fc-ac-OMPA/MWCNTs layer (Fig. 4C). This figure highlights the existence of five major peaks corresponding to the following elements: Fe at 709 eV, C at 287 eV, O at 537 eV and N at 402 eV. After the DNA probe grafting, we noted the enlargement and the shifting of the Nitrogen (N) peak's (Fig. 4D). This can be explained by the fact that DNA is rich in amino groups in its chemical structure with a high coverage of DNA on the nanocomposite layer [45]. Moreover, the appearance of a new peak at 136 eV corresponds to the phosphorus element (P) which is present only in the DNA chain (Fig. 4E). These XPS analyses are in good agreement with the electrochemical measurements and confirm the good grafting of the DNA on the nanocomposite membrane.

After the DNA probe grafting step, we have proceeded with the hybridization of the complementary target (c DNA) by incubating the modified electrode in a solution of 1 fmol L^{-1}, 10 fmol L^{-1}, 100 fmol L^{-1}, 1 pmol L^{-1}, 10 pmol L^{-1}, 100 pmol L^{-1} and 1 nmol L^{-1}, respectively, for 1 h at 40 °C. Fig. 5A shows the subsequent hybridization of each concentration by cyclic voltammetry. It has been noted that when the concentration of the complementary DNA increases, the redox signal decreases with a shift of the potentials towards the positive potentials. This decrease is proportional to the specific binding of the amine group of the probe to its target immobilized on the surface. In fact, attachment of large DNA molecules affects more the redox signal of the ferrocene groups' which lead to the slow diffusion of ions to the surface during the redox process [43]. This behavior has also been observed in our previous work based on another redox polymer Fc-PPP/MWCNT's [26]. This decrease starts from 1 fmol L^{-1} with a variation of 28%, suggesting a high sensitivity of this biosensor. However, the incubation of the biosensor with a highly concentrated solution (1 nmol L^{-1}) of non-complementary (nc DNA) target resulted in a weak signal variation of 30% compared to the same concentration of c DNA with a greater variation of 90% (Fig. 5B). This large current decrease with the DNA target concentration suggests that almost all carboxylic groups immobilized were associated with the DNA [46]. The slight variation of nc DNA may result from the non-specific adsorption on the biosensor surface due to the hydrophobicity of the CNTs [47]. Nevertheless, a wide difference of 60% between the c DNA and the nc DNA response confirms the good selectivity of our biosensor. It is then contemplated to improve it by associating it with some agent that prevents

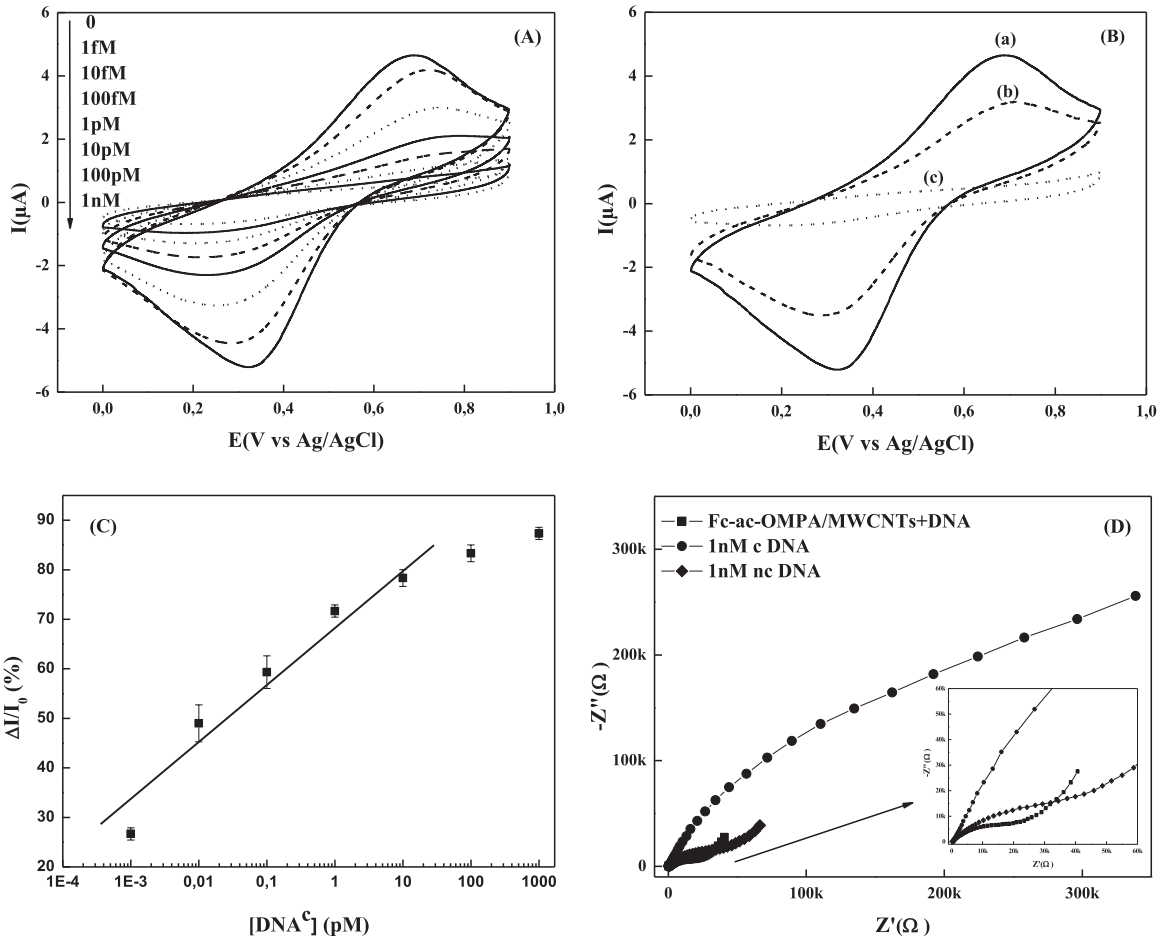

Fig. 5. (A) CV of biosensors obtained after DNA target hybridization at various concentrations from 1 fM to 1 nM. (B) CV presents the results obtained for non-specific interactions compared to specific one. Curve (a) Fc-ac-OMPA/MWCNTs + DNA, curve (b) Fc-ac-OMPA/MWCNTs + 1 nM ncDNA, and curve (c) Fc-ac-OMPA/MWCNTs + 1 nM cDNA. The hybridization was performed in PBS (pH = 7.4) during 1 h at 40 °C. The CVs are recorded in 0.1 M $LiClO_4$ (pH = 7) with scan rate of 50 mV s^{-1}. (C) Plot of the calibration curve presenting the relative variation of the current peak versus concentration of DNA target at logarithm scale, where I_0 is the peak current corresponding to DNA probe response and ΔI is the response of each incubation of DNA target concentration. (B) Nyquist plots recorded at 0.45 V vs Ag/AgCl in the frequency range of 100 kHz to 100 mHz. (■) Fc-ac-OMPA/MWCNTs + DNA, (▲) Fc-ac-OMPA/MWCNTs + DNA + 1 nM ncDNA, (•) Fc-ac-OMPA/MWCNTs + DNA + 1 nM cDNA. The points presenting the experimental data and the line is the fit obtained with the equivalent circuit. Right is the zoom of diagram at lower frequency range.

non-specific interaction, such as polyethylene glycol or anionic polymer that will prevent this adsorption and improve the selectivity. EIS measurements were also performed to study the selectivity of the biosensor with the nc DNA target. The fitting of the experimental Nyquist at high concentration of 1 nmol L^{-1} for both c DNA and nc DNA, demonstrates an important value of the charge transfer resistance with c DNA (Rct = 309.18 kΩ). That may be due to an increase in the negative charges of the biolayer [48]. On the other side, the charge transfer resistance of the non-complementary (nc DNA) is lower (Rct = 46.32 kΩ) (Fig. 5D). These results are consistent with cyclic voltammetry results and confirm that our biosensor is specific.

Based on the changes of current corresponding to redox signal of ferrocene, obtained after incubation of the biosensor with each c DNA concentration, the calibration curve was plotted (Fig. 5C). This curve is represented in logarithmic scale in order to demonstrate the large dynamic range of detection from 1 fmol L^{-1} to 10 pmol L^{-1}. The broadening of the dynamic range compared to that of the pure redox oligomer Fc-ac-OMPA confirms the large surface area of our nanocomposite layer thanks to the insertion of the CNTs with the redox oligomer. The detection limit based on signal-to-noise ratio of 3 has been calculated by using the formula 3σ/s, where σ is the standard deviation and s is the slope of the calibration curve. The detection limit was found equal to 0.08 fmol L^{-1}. These measurements were highly reproducible; where the standard deviation of 1.25–3.74% for 3 independent measurements has been obtained. This LOD obtained is highly better than that reported with our previous work Fc-PPP/MWCNTs (detection range of 1 fmol L^{-1} to 10 pmol L^{-1}, LOD = 1.6 pmol L^{-1}) [26] and Fc-ac-OMPA (detection range of 1 fmol L^{-1} to 100 pmol L^{-1}, LOD = 0.2 fmol L^{-1}) [22]. Also, this LOD is better compared to the LOD value obtained for biosensors using conducting polymer without redox mediator on its chain, we can site, for example nanomaterials based on (MWCNTs/PPy/PAMAM) (detection range from 1 fmol L^{-1} to 100 nmol L^{-1}, LOD = 0.3 fmol L^{-1}) [43] and the p-Aminobenzoicacid (PABA) / SWNTCs membrane (detection range from 1 pmol L^{-1} to 0.1 µmol L^{-1}, LOD = 35 pmol L^{-1}) [48]. Comparing previous works with ours, we can highlight the good electrochemical properties of our nanocomposite transducer Fc-ac-OMPA/MWCNTs. We have gained in sensitivity and in the ease of fabrication without any further steps as indicated in other redox polymer or conducting polymer.

3.4. DNA detection from clinical samples of drug resistant Mycobacterium Tuberculosis

We have tested the performance of our nanocomposite biosensor Fc-ac-OMPA/MWCNTs with the genomic DNA of *M. tuberculosis* and we proceeded in the same way presented for the synthetic Hepatitis C DNA. The *M.Tuberculosis* probe (1 µmol L^{-1}) has been denaturized by heating

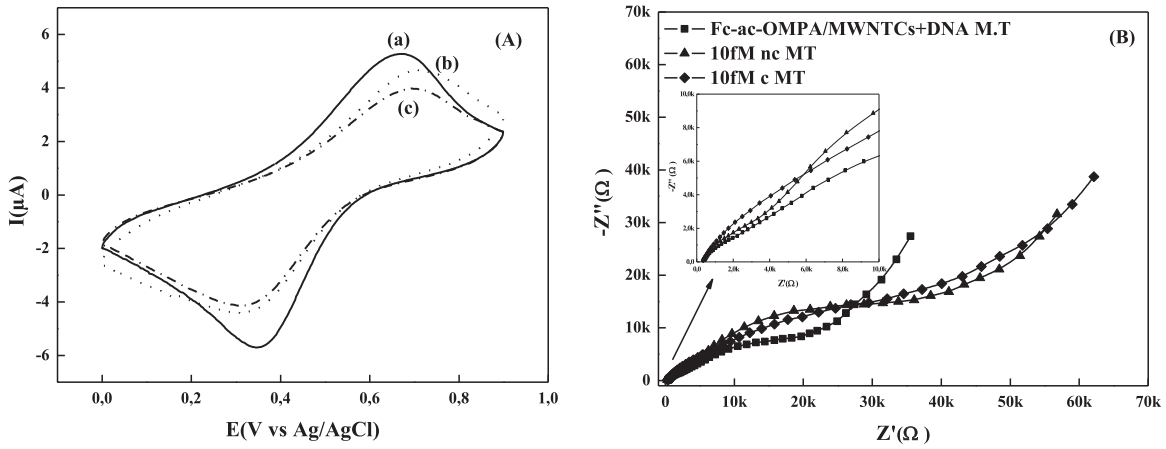

Fig. 6. (A) CV presents the results obtained for mutant and wild M.T attachment. Curve (a) Fc-ac-OMPA/MWCNTs + M.T probe, curve (b) Fc-ac-OMPA/MWCNTs + probe + 10 fM ncM.T, and curve (c) Fc-ac-OMPA/MWCNTs + probe + 10 fM cM.T. The CVs are recorded in 0.1 M $LiClO_4$ (pH = 7) with scan rate of 50 mV s^{-1}. (B) Nyquist plots recorded at 0.45 V vs Ag/AgCl in the frequency range of 100 kHz to 100 mHz. (■) Fc-ac-OMPA/MWCNTs + M.Tprobe, (▲) Fc-ac-OMPA/MWCNTs + probe + 10fM ncM.T, (•) Fc-ac-OMPA/MWCNTs + probe + 10fM cM.T. The points presenting the experimental data and the line is the fit obtained with the equivalent circuit. Left is the zoom of diagram at lower frequency range.

at 95 °C for 4 min. Next the DNA was anchored on the modified nanocomposite electrode followed by a blocking step of the non-active sites with ethanolamine. The biosensors were then analyzed using CV and EIS techniques. The decrease of the ferrocene signal and the increase of the charge transfer resistance after the attachment of the DNA probe on the nanocomposite membrane with a value Rct = 37.89 kΩ has been observed. This indicates the successful grafting of the probe by a covalent attachment to the Fc-ac-OMPA/MWCNTs membrane. The hybridization reaction with either wild sequence (c M.T) or with the mutant sequence (nc M.T) has been performed separately with the concentration of 10 fmol L^{-1}. The voltammogram obtained showed a decrease of the ferrocene signal of 26% for the wild and 11% for the mutated (Fig. 6A). Moreover, on the basis of the EIS results, the charge transfer resistance after hybridization of the wild (c M.T) is slightly greater than that of the mutated DNA (nc M.T) with values of Rct = 68.08 kΩ and Rct = 57.52 kΩ respectively (Fig. 6B). These results, after the *Mycobacterium tuberculosis* strain hybridization, show that our biosensor based on the new redox oligomer Fc-ac-OMPA doped by MWCNTs is able to discriminate the hybridization of wild and mutant samples which differ by only a single mutation (T**C**G/T**T**G). To further verify the selectivity of this biosensor, other DNA sequences can be used by varying the length or the number of mutations in the resistant DNA and see if more sensitive variations can be obtained. These results are comparable to those demonstrated in the literature with other types of biosensors based on carbon nanotubes modified with ferrocene where the biosensor is integrated into a microfluidic platform [49]. Although, we have compared these results to our previous work with only the redox polymer Fc-ac-OMPA [22]. We noticed a better sensibility and selectivity. This confirms the effect of doping redox oligomer with MWCNTs that offer a larger surface-to-volume ratio and exhibits their electrochemical properties for the use of the biosensor devices. These results prove that this kind of nanocomposite based on redox oligomer allows the obtaining of a good performance regarding DNA sensing from a PCR amplification with direct patterning and without further treatment.

4. Conclusion

In this work, a new approach has been proposed for the electrochemical detection of DNA with a novel nanocomposite membrane based on a novel redox oligomer (Fc-ac-OMPA). For this purpose, the morphological and surface properties of this nanocomposite deposited on the gold surface have been studied, where it has been confirmed that this membrane is well suited for grafting the biolayer. The presence of the COOH groups grafted onto the redox oligomer chain allows the direct anchoring of the biolayer, which was confirmed by XPS. Comparing the electrochemical response of the two biosensors based on the redox oligomer alone and the nanocomposite membrane, it has been concluded that the nanocomposite membrane has improved the anchoring of the DNA strands. This amelioration has further increased the sensitivity of our biosensor as well as the dynamic range (1 fmol L^{-1} to1 nmol L^{-1}). Moreover the biosensor based on Fc-ac-OMPA/MWCNTs has shown appreciable sensitivity to real samples of the DNA from *Mycobacterium tuberculosis*. This biosensor demonstrates a potential in its application for DNA sensing and is able to discriminate SNP mutation coming from strand with drug resistance. The easy construction of this biosensor, besides its good reproducibility and very low time consuming, make this nanocomposite Fc-ac-OMPA/MWCNTs very highly competitive for further application in pathogens diagnostic and therapeutic purpose.

Acknowledgments

We would like to thank Professor C. Sola from “laboratory I2BC”, University of Paris-Sud for providing the *M.Tuberculosis samples*. We would like to thank also ICMMO and LPN engineers' platforms for measurements of XPS and SEMs images.

Appendix A. Supporting information

Supplementary data associated with this article can be found in the online version at http://dx.doi.org/10.1016/j.talanta.2018.03.025.

References

[1] E. Torres-Chavolla, E.C. Alocilja, Aptasensors for detection of microbial and viral pathogens, Biosens. Bioelectron. 24 (2009) 3175–3182, http://dx.doi.org/10.1016/j.bios.2008.11.010.

[2] M. Arentz, T.R. Hawn, Tuberculosis infection: insight from immunogenomics, Drug Discov. Today Dis. Mech. 4 (2007) 231–236, http://dx.doi.org/10.1016/j.ddmec.2007.11.003.

[3] M. Caws, S.M. Wilson, C. Clough, F. Drobniewski, Role of IS6110-targeted PCR, culture, biochemical, clinical, and immunological criteria for diagnosis of tuberculous meningitis, J. Clin. Microbiol. 38 (2000) 3150–3155.

[4] K.K.R. Steingart, V. Ng, M. Henry, P.C. Hopewell, A. Ramsay, J. Cunningham, R. Urbanczik, M.D. Perkins, M.A. Aziz, M. Pai, Sputum processing methods to improve the sensitivity of smear microscopy for tuberculosis: a systematic review, Lancet Infect. Dis. 6 (2006) 664–674, http://dx.doi.org/10.1016/S1473-3099(06)70602-8.

[5] R. Sanjuan-Jimenez, P. Morata, P. Bermudez, M.J. Bravo, J.D. Colmenero, Comparative clinical study of different multiplex real time PCR strategies for the simultaneous differential diagnosis between extrapulmonary tuberculosis and focal complications of brucellosis, PLoS Negl. Trop. Dis. 7 (2013) e2593, http://dx.doi.

org/10.1371/journal.pntd.0002593.
[6] M. Fukushima, K. Kakinuma, H. Hayashi, H. Nagai, K. Ito, R. Kawaguchi, Detection and identification of Mycobacterium species isolates by DNA microarray detection and identification of mycobacterium species isolates by DNA microarray, J. Clin. Microbiol. 41 (2003) 2605–2615, http://dx.doi.org/10.1128/JCM.41.6.2605.
[7] R. Pahwa, S. Hedau, S. Jain, N. Jain, V.M. Arora, N. Kumar, B.C. Das, Assessment of possible tuberculous lymphadenopathy by PCR compared to non-molecular methods, J. Med. Microbiol. 54 (2005) 873–878, http://dx.doi.org/10.1099/jmm.0.45904-0.
[8] Y. Zhang, P. Ozdemir, Microfluidic, DNA amplification-a review, Anal. Chim. Acta 638 (2009) 115–125, http://dx.doi.org/10.1016/j.aca.2009.02.038.
[9] C. Lui, N.C. Cady, C.A. Batt, Nucleic acid-based detection of bacterial pathogens using integrated microfluidic platform systems, Sensors (Basel) (2009), http://dx.doi.org/10.3390/s90503713.
[10] M.U. Ahmed, S. Nahar, M. Safavieh, M. Zourob, Real-time electrochemical detection of pathogen DNA using electrostatic interaction of a redox probe, Analyst 138 (2013) 907–915, http://dx.doi.org/10.1039/C2AN36153A.
[11] L. Zhu, R. Zhao, K. Wang, H. Xiang, Z. Shang, W. Sun, Electrochemical behaviors of methylene blue on DNA modified electrode and its application to the detection of PCR product from NOS sequence, Sensors 8 (2008) 5649–5660, http://dx.doi.org/10.3390/s8095649.
[12] B. Ferguson, S. Buchsbaum, Integrated microfluidic electrochemical DNA sensor, Anal. Chem. 81 (2009) 6503–6508, http://dx.doi.org/10.1021/ac900923e.
[13] R.H. Liu, J. Yang, R. Lenigk, J. Bonanno, P. Grodzinski, Self-contained, fully integrated biochip for sample preparation, polymerase chain reaction amplification, and DNA microarray detection, Anal. Chem. 76 (2004) 1824–1831, http://dx.doi.org/10.1021/ac0353029.
[14] E. Torres-Chavolla, E.C. Alocilja, Nanoparticle based DNA biosensor for tuberculosis detection using thermophilic helicase-dependent isothermal amplification, Biosens. Bioelectron. 26 (2011) 4614–4618, http://dx.doi.org/10.1016/j.bios.2011.04.055.
[15] H. Qi, X. Li, P. Chen, C. Zhang, Electrochemical detection of DNA hybridization based on polypyrrole/ss-DNA/multi-wall carbon nanotubes paste electrode, Talanta 72 (2007) 1030–1035, http://dx.doi.org/10.1016/j.talanta.2006.12.032.
[16] P. Jolly, P. Zhurauski, J.L. Hammond, A. Miodek, S. Liébana, T. Bertok, J. Tkáč, P. Estrela, Self-assembled gold nanoparticles for impedimetric and amperometric detection of a prostate cancer biomarker, Sens. Actuat. B Chem. 251 (2017) 637–643, http://dx.doi.org/10.1016/j.snb.2017.05.040.
[17] W.T. Lu and, Cuichen Peng, Mingxu Wu, Da You, Yan Han, Ting Chen, Mao Fu, M. Ye, Engineering and applications of DNA-grafting polymer materials, Chem. Sci. 4 (2013) 1928–1938, http://dx.doi.org/10.1039/C2SC21198J.
[18] F. Kuralay, A. Erdem, S. Abaci, H. Özyörük, A. Yildiz, Poly(vinylferrocenium) coated disposable pencil graphite electrode for DNA hybridization, Electrochem. Commun. 11 (2009) 1242–1246, http://dx.doi.org/10.1016/j.elecom.2009.04.010.
[19] R. Ayranci, D.O. Demirkol, M. Ak, S. Timur, Ferrocene-functionalized 4-(2,5-Di (thiophen-2-yl) − 1H-pyrrol-1- yl)aniline: a novel design in conducting polymer-based electrochemical biosensors, Sensors (Switzerland) 15 (2015) 1389–1403, http://dx.doi.org/10.3390/s150101389.
[20] A. Miodek, G. Castillo, T. Hianik, H. Korri-Youssoufi, Electrochemical aptasensor of human cellular prion based on multiwalled carbon nanotubes modified with dendrimers: a platform for connecting redox markers and aptamers, Anal. Chem. 85 (2013) 7704–7712, http://dx.doi.org/10.1021/ac400605p.
[21] S. Bizid, R. Mlika, A. Haj Said, M. Chemli, H. Korri Youssoufi, Investigations of poly (p-phenylene) modified with ferrocene and their application in electrochemical DNA sensing, Sens. Actuat. B Chem. 226 (2016) 370–380, http://dx.doi.org/10.1016/j.snb.2015.11.137.
[22] S. Bizid, S. Blili, R. Mlika, A. Haj Said, H. Korri-Youssoufi, Direct electrochemical DNA Sensor based on a new redox oligomer modified with ferrocene and carboxylic acid: application to the detection of Mycobacterium tuberculosis mutant strain, Anal. Chim. Acta 994 (2017) 10–18, http://dx.doi.org/10.1016/j.aca.2017.09.022.
[23] A.T. Dimitrov, A. Tomova, A. Grozdanov, O. Popovski, P. Paunović, Electrochemical production, characterization, and application of MWCNTs, J. Solid State Electrochem. 17 (2013) 399–407, http://dx.doi.org/10.1007/s10008-012-1896-z.
[24] M. Pumera, S. Sánchez, I. Ichinose, J. Tang, Electrochemical nanobiosensors, Sens. Actuat. B Chem. 123 (2007) 1195–1205, http://dx.doi.org/10.1016/j.snb.2006.11.016.
[25] T. Yang, W. Zhang, M. Du, K. Jiao, A PDDA/poly(2,6-pyridinedicarboxylic acid)-CNTs composite film DNA electrochemical sensor and its application for the detection of specific sequences related to PAT gene and NOS gene, Talanta 75 (2008) 987–994, http://dx.doi.org/10.1016/j.talanta.2007.12.049.
[26] S. Bizid, R. Mlika, A. Haj Saïd, M. Chemli, H. Korri Youssoufi, Functionalization of MWCNTs with ferrocene-poly(p-phenylene) and effect on electrochemical properties: application as a sensing platform, Electroanalysis 28 (2016) 2533–2542, http://dx.doi.org/10.1002/elan.201600142.
[27] E. Granot, B. Basnar, Z. Cheglakov, E. Katz, I. Willner, Enhanced bioelectrocatalysis using single-walled carbon nanotubes (SWCNTs)/polyaniline hybrid systems in thin-film and microrod structures associated with electrodes, Electroanalysis 18 (2006) 26–34, http://dx.doi.org/10.1002/elan.200503403.
[28] A. Noll, T. Burkhart, Morphological characterization and modelling of electrical conductivity of multi-walled carbon nanotube/poly(p-phenylene sulfide) nanocomposites obtained by twin screw extrusion, Compos. Sci. Technol. 71 (2011) 499–505, http://dx.doi.org/10.1016/j.compscitech.2010.12.026.
[29] A. Benvidi, N. Rajabzadeh, M. Mazloum-Ardakani, M.M. Heidari, Comparison of impedimetric detection of DNA hybridization on chemically and electrochemically functionalized multi-wall carbon nanotubes modified electrode, Sens. Actuat. B Chem. 207 (2015) 673–682, http://dx.doi.org/10.1016/j.snb.2014.10.043.
[30] S. Blili, Z. Zaâboub, H. Maaref, A. Haj Said, Synthesis of a new π-conjugated redox oligomer: electrochemical and optical investigation, J. Mol. Struct. 1128 (2017) 111–116, http://dx.doi.org/10.1016/j.molstruc.2016.08.045.
[31] M.K. Gomgnimbou, E. Abadia, J. Zhang, G. Refrégier, S. Panaiotov, E. Bachiyska, C. Sola, "Spoligoriftyping," a dual-priming-oligonucleotide-based direct-hybridization assay for tuberculosis control with a multianalyte microbead-based hybridization system, J. Clin. Microbiol. 50 (2012) 3172–3179, http://dx.doi.org/10.1128/JCM.00976-12.
[32] I. Bergval, S. Sengstake, N. Brankova, V. Levterova, E. Abadía, N. Tadumaze, N. Bablishvili, M. Akhalaia, K. Tuin, A. Schuitema, S. Panaiotov, E. Bachiyska, T. Kantardjiev, R. de Zwaan, A. Schürch, D. van Soolingen, A. van't Hoog, F. Cobelens, R. Aspindzelashvili, C. Sola, P. Klatser, R. Anthony, Combined species identification, genotyping, and drug resistance detection of mycobacterium tuberculosis cultures by mlpa on a bead-based array, PLoS One 7 (2012) e43240, http://dx.doi.org/10.1371/journal.pone.0043240.
[33] J. Yang, T. Xu, A. Lu, Q. Zhang, H. Tan, Q. Fu, Preparation and properties of poly (p-phenylene sulfide)/multiwall carbon nanotube composites obtained by melt compounding, Compos. Sci. Technol. 69 (2009) 147–153, http://dx.doi.org/10.1016/j.compscitech.2008.08.030.
[34] J. Zeng, W. Wei, L. Wu, X. Liu, K. Liu, Y. Li, Fabrication of poly(toluidine blue O)/carbon nanotube composite nanowires and its stable low-potential detection of NADH, J. Electroanal. Chem. 595 (2006) 152–160, http://dx.doi.org/10.1016/j.jelechem.2006.07.014.
[35] K. Yang, B. Xing, Adsorption of organic compounds by carbon nanomaterials in aqueous phase: Polanyi theory and its application, Chem. Rev. 110 (2010) 5989–6008, http://dx.doi.org/10.1021/cr100059s.
[36] X. Mao, G.C. Rutledge, T.A. Hatton, Polyvinylferrocene for noncovalent dispersion and redox-controlled precipitation of carbon nanotubes in nonaqueous media, Langmuir 29 (2013) 9626–9634, http://dx.doi.org/10.1021/la401440w.
[37] G.D. Costanzo, S. Ledesma, I. Mondragon, S. Goyanes, Stable solutions of multi-walled carbon nanotubes using an azobenzene dye, J. Phys. Chem. C 114 (2010) 14347–14352, http://dx.doi.org/10.1021/jp102580b.
[38] K. Jagadish, S. Srikantaswamy, K. Byrappa, L. Shruthi, M.R. Abhilash, Dispersion of multiwall carbon nanotubes in organic solvents through hydrothermal supercritical condition, J. Nanomater. 2015 (2015) 1–6, http://dx.doi.org/10.1155/2015/381275.
[39] S.A. Kumar, S.F. Wang, T.C.K. Yang, C.T. Yeh, Acid yellow 9 as a dispersing agent for carbon nanotubes: preparation of redox polymer-carbon nanotube composite film and its sensing application towards ascorbic acid and dopamine, Biosens. Bioelectron. 25 (2010) 2592–2597, http://dx.doi.org/10.1016/j.bios.2010.04.024.
[40] V. Brânzoi, F. Brânzoi, L. Pilan, N. Donisan, The characterization of some nanocomposites based on conducting polymers and carbon nanotubes obtained by co-polymerization, Rev. Roum. Chim. 55 (2010) 369–378.
[41] J.E.B. Randles, Kinetics of rapid electrode reactions, Discuss. Faraday Soc. 1 (1947) 11, http://dx.doi.org/10.1039/df9470100011.
[42] E. Laviron, General expression of the linear potential sweep voltammogram in the case of diffusionless electrochemical systems, J. Electroanal. Chem. 101 (1979) 19–28, http://dx.doi.org/10.1016/S0022-0728(79)80075-3.
[43] A. Miodek, N. Mejri, M. Gomgnimbou, C. Sola, H. Korri-Youssoufi, E-DNA sensor of mycobacterium tuberculosis based on electrochemical assembly of nanomaterials (MWCNTs/PPy/PAMAM), Anal. Chem. 87 (2015) 9257–9264, http://dx.doi.org/10.1021/acs.analchem.5b01761.
[44] N. Prabhakar, K. Arora, S.P. Singh, M.K. Pandey, H. Singh, B.D. Malhotra, Polypyrrole-polyvinyl sulphonate film based disposable nucleic acid biosensor, Anal. Chim. Acta 589 (2007) 6–13, http://dx.doi.org/10.1016/j.aca.2007.01.084.
[45] D.Y. Petrovykh, H. Kimura-Suda, L.J. Whitman, M.J. Tarlov, Quantitative analysis and characterization of DNA immobilized on gold, J. Am. Chem. Soc. 125 (2003) 5219–5226, http://dx.doi.org/10.1021/ja029450c.
[46] H.Q.A. Lê, S. Chebil, B. Makrouf, H. Sauriat-Dorizon, B. Mandrand, H. Korri-Youssoufi, Effect of the size of electrode on electrochemical properties of ferrocene-functionalized polypyrrole towards DNA sensing, Talanta 81 (2010) 1250–1257, http://dx.doi.org/10.1016/j.talanta.2010.02.017.
[47] V. Chan, D.J. Graves, P. Fortina, S.E. Mckenzie, Adsorption and surface diffusion of DNA oligonucleotides at liquid / solid interfaces, Langmuir 28 (1997) 320–329, http://dx.doi.org/10.1021/la960670b.
[48] M. Wang, W. Gong, Q. Meng, Y. Zhang, Electrochemical DNA impedance biosensor for the detection of DNA hybridization with polymeric film, single walled carbon nanotubes modified glassy carbon electrode, Russ. J. Electrochem. 47 (2011) 1368–1373, http://dx.doi.org/10.1134/S1023193511120123.
[49] B. Zribi, E. Roy, A. Pallandre, S. Chebil, M. Koubaa, N. Mejri, H. Magdinier Gomez, C. Sola, H. Korri-Youssoufi, A.M. Haghiri-Gosnet, A microfluidic electrochemical biosensor based on multiwall carbon nanotube/ferrocene for genomic DNA detection of Mycobacterium tuberculosis in clinical isolates, Biomicrofluidics 10 (2016), http://dx.doi.org/10.1063/1.4940887.